THE JOURNAL OF PHYSICAL CHEMISTRY A

ARTICLE

pubs.acs.org/JPCA

Reaction-Induced Magnetic Transition in Mn_2 Dimers

Miao Miao Wu,[†,‡] Qian Wang,[†] Qiang Sun,[‡,†] and Puru Jena[*,†]

[†]Department of Physics, Virginia Commonwealth University, Richmond, Virginia 23284, United States

[‡]Department of Advanced Materials and Nanotechnology, and Center for Applied Physics and Technology, Peking University, Beijing 100871, China

ABSTRACT: The magnetic coupling between Mn atoms in Mn_2 dimers embedded in a rare gas matrix is antiferromagnetic but undergoes ferromagnetic transition at a higher temperature or when ionized to the Mn_2^+ state. By use of density functional theory and hybrid functional for exchange-correlation potentials, we show that ferromagnetic transition can also be induced when Mn_2 reacts with Cl and/or BO_2. Because of their highly electronegative character, both Cl and BO_2 draw electrons from the Mn_2 dimer leaving it in a positively charged state. The resulting shrinkage in the Mn−Mn bond brought about by the removal of an antibonding electron causes the magnetic transition. We further show that the coupling between Mn atoms remains ferromagnetic when two Mn_2Cl units are allowed to interact with each other. The ability to induce a magnetic transition through a chemical reaction provides a way to synthesize new magnetic materials.

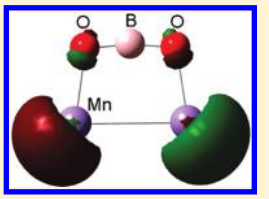

I. INTRODUCTION

Manganese is a unique element in the 3d transition metal series. With an electronic configuration of half-filled 3d and filled 4s shells ($3d^5\ 4s^2$), the Mn atom forms the weakest dimer with the longest bond among all elements in the early transition metal series.[1] For the same reason its bulk crystal also has the lowest cohesive energy.[1,2] Electrons in the half-filled $3d^5$ shell are fairly localized compared to other transition metal atoms, and the Mn atom possesses a magnetic moment of 5 μ_B. Both the Mn_2 dimer and Mn crystal are antiferromagnetic.[3−7] On the other hand, Mn atoms in small clusters containing less than 5 atoms are ferromagnetic, and the coupling turns into ferri- or antiferromagnetic as the cluster size increases.[8,9] It has also been found that when an electron is removed from Mn_2 dimer the resulting Mn_2^+ cation becomes ferromagnetic with a magnetic moment of 11 μ_B.[10−13] Since the magnetic moment of Mn and its magnetic properties can be influenced by their environment it has always been of interest to find ways to induce ferromagnetic coupling between Mn atoms.

In this work, we show that the antiferromagnetic coupling between Mn atoms in Mn_2 dimer can be made ferromagnetic by reacting with electronegative species such as Cl and BO_2. Our hypothesis is that an electronegative species would draw an electron from the Mn_2 dimer leaving it in a Mn_2^+ state, and hence the compound system can be ferromagnetic with a magnetic moment of 11 μ_B. To verify this hypothesis, we chose Cl and BO_2 moiety as reactants. Chlorine has the highest electron affinity, namely, 3.6 eV among all elements in the periodic table. With an extra electron Cl^- forms a stable closed shell ion following the octet rule. BO_2^-, on the other hand, is isoelectronic with CO_2, and it too forms a closed shell when the extra electron is attached to BO_2. The electron affinity of BO_2, namely, 4.46 eV,[14] is even larger than that of Cl and is referred to as a superhalogen.[15,16] We calculated the equilibrium geometry of Mn_2Cl and Mn_2BO_2 for both neutral and anionic states for all possible spin configurations using density functional theory. The ground state of the neutral clusters is found to be ferromagnetic with a total magnetic moment of 11 μ_B, which is equally shared between the two Mn atoms. To see if the coupling between Mn atoms remain ferromagnetic when clusters grow, we calculated the geometries and preferred spin configurations of $(Mn_2Cl)_2$. The total magnetic moment of such a system is found to be 18 μ_B, and all Mn atoms are ferromagnetically coupled. We have computed the vertical detachment energies and electron affinities of Mn_2Cl, Mn_2BO_2, and $(Mn_2Cl)_2$ so that our predictions can later be compared with photoelectron spectroscopy experiments to verify the accuracy of our theoretical approach. In section II we describe the theoretical procedure. Results are presented and discussed in section III and summarized in section IV.

Table 1. IPs, EAs, and Magnetic Moments (MM) of Mn and Cl Atoms Calculated Using Different Exchange-Correlation Energy Functionals and 6-311+G* Basis Set

Mn				Cl		
level of theory	IP (eV)	EA (eV)	MM (μ_B)	level of theory	IP (eV)	EA (eV)
B3LYP	7.52	0.60	5	B3LYP	13.07	3.72
BPW91	6.34	0.68	5	BPW91	12.98	3.67
PBE	6.31	0.84	5	PBE	12.97	3.70
LSDA	7.96	0.84	5	LSDA	13.73	4.46
exptl	7.43	NA	5	exptl	12.96	3.61

Received: July 5, 2010
Revised: November 3, 2010
Published: December 29, 2010

Table 2. Atomic Spin from Mulliken Analysis Using Three Different Functionals (B3LYP, HSE, LC-ωPBE), Atomic Charge from Natural Bond Orbital (NBO) Analysis, Total Magnetic Moment (MM), EA, Highest-Occupied Molecular Orbital (HOMO)−Lowest-Unoccupied Molecular Orbtial (LUMO) Gaps and Symmetry of Clusters Studied

		Mulliken atomic spin (μ_B)						
clusters (symmetry)	atom	B3LYP	HSE	LC-ωPBE	NBO charges	MM (μ_B)	EA (eV)	gap (eV)
MnCl ($C_{\infty v}$)	Mn	5.84	5.90	5.90	0.75	6	1.57	2.26
	Cl	0.16	0.10	0.10	−0.75			
$MnCl^-$ ($C_{\infty v}$)	Mn	4.91	4.92	4.95	−0.10	5		2.55
	Cl	0.09	0.08	0.05	−0.90			
Mn_2Cl (C_{2v})	1 Mn	5.44	5.46	5.47	0.40	11	1.40	2.20
	2 Mn	5.44	5.46	5.47	0.40			
	Cl	0.12	0.08	0.06	−0.80			
Mn_2Cl^- ($D_{\infty h}$)	1 Mn	4.94	4.90	4.90	−0.08	0		2.79
	2 Mn	−4.94	−4.90	−4.90	−0.08			
	3 Cl	0.00	0.00	0.00	−0.82			
$MnBO_2$ ($C_{\infty v}$)	1 B	−0.01	−0.01	0.00	1.19	6	2.00	2.44
	2 O	−0.02	−0.06	−0.06	−1.22			
	3 O	−0.02	0.01	0.01	−0.86			
	4 Mn	6.02	6.06	6.05	0.89			
$MnBO_2^-$ ($C_{\infty v}$)	1 B	0.03	0.03	0.01	1.17	5		2.71
	2 O	0.01	−0.01	−0.03	−1.20			
	3 O	−0.01	−0.01	−0.01	−0.95			
	4 Mn	4.97	4.99	5.03	−0.02			
Mn_2BO_2 (C_{2v})	1 O	0.00	−0.02	−0.02	−1.04	11	1.78	2.07
	2 O	0.00	−0.02	−0.02	−1.04			
	3 Mn	5.45	5.46	5.46	0.46			
	4 Mn	5.45	5.46	5.46	0.46			
	5 B	0.10	0.12	0.12	1.16			
$Mn_2BO_2^-$ ($D_{\infty h}$)	1 O	−0.01	−0.01	−0.01	−1.09	0		3.51
	2 O	0.01	0.01	0.01	−1.09			
	3 Mn	4.99	5.00	4.99	−0.05			
	4 Mn	−4.99	−5.00	−4.99	−0.05			
	5 B	0.00	0.00	0.00	1.27			
$(Mn_2Cl)_2$ (C_s)	1 Mn	4.57	4.58	4.42	0.39	18	1.74	1.73
	2 Cl	0.03	−0.01	0.01	−0.73			
	3 Mn	4.37	4.36	4.39	0.38			
	4 Mn	4.34	4.34	4.53	0.27			
	5 Cl	0.04	0.00	0.01	−0.71			
	6 Mn	4.65	4.73	4.64	0.40			
$(Mn_2Cl)_2^-$ (C_{2h})	1 Mn	5.04	5.05	5.01	−0.01	19		1.45
	2 Mn	4.43	4.45	4.47	0.30			
	3 Mn	5.04	5.05	5.01	−0.01			
	4 Cl	0.02	0.00	0.02	−0.79			
	5 Mn	4.43	4.45	4.47	0.30			
	6 Cl	0.02	0.00	0.02	−0.79			

II. THEORETICAL PROCEDURES

Our calculations are carried out using density functional theory (DFT) and Becke's three parameter hybrid exchange functional and the Lee−Yang−Par correlation functional (B3LYP)[17−19] for the exchange-correlation potential. The all-electron 6-311+G* basis set implemented in the GAUSSIAN 03 code were used in all the calculations.[20] Ionization potentials (IPs) and electron affinities (EAs) of Mn and Cl atoms were used to bench mark the best functional (B3LYP, BPW91, PBE, and LSDA) for the calculations.[21−23] From the results given in Table 1, we note that the B3LYP hybrid functional and 6-311+G* basis set provide the best agreement with the experimental data. It has also been shown from previous calculations that the hybrid functionals, especially the hybrid B3LYP functional combined with the broken-symmetry approach, yields the most reliable magnetic exchange couplings.[19,24−27] To compare with our results based on B3LYP, we have carried out calculations of the atomic spin populations for all the clusters using two other hybrid functionals, namely, the short-range separated Heyd−Scuseria−Ernzerhof (HSE) functional and the long-range

dx.doi.org/10.1021/jp106198u |J. Phys. Chem. A 2011, 115, 549–555

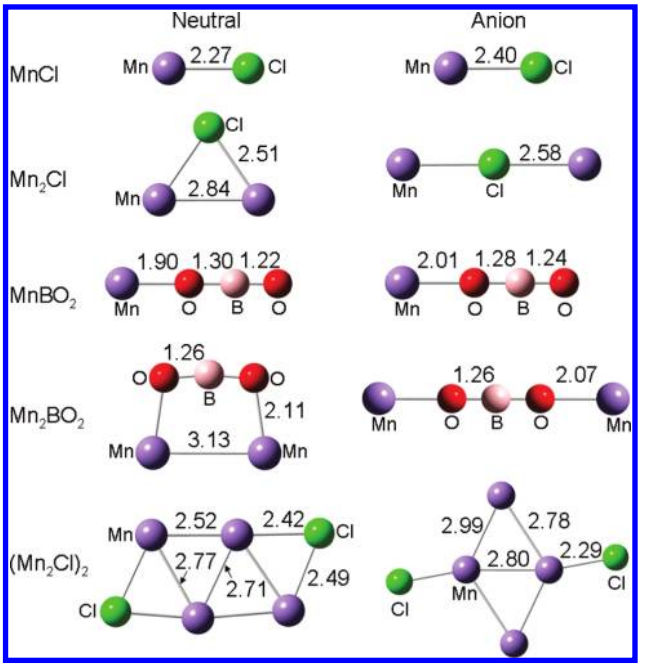

Figure 1. The optimized geometries of neutral (left column) and anionic (right column) clusters of MnCl, Mn_2Cl, $MnBO_2$, Mn_2BO_2, and $(Mn_2Cl)_2$.

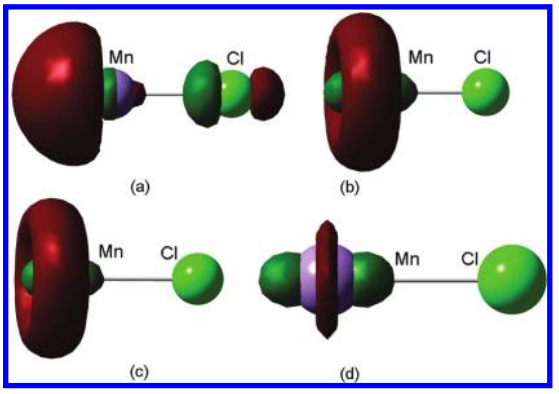

Figure 2. (a) HOMO and (b) LUMO of MnCl; (c) HOMO and (d) LUMO of $MnCl^-$.

corrected (LC-ωPBE) functional.[28,29] These are summarized in Table 2. We see that the results agree with each other very well (see the comparison in Table 2). Therefore, the B3LYP functional can yield quite reliable results in this particular case.

Hence, all calculations were carried out using the B3LYP functional and the 6-311+G* basis set implemented in the GAUSSIAN 03 code. The geometries were optimized without any symmetry constraint. For each cluster several initial structures were used to ensure that the lowest-energy structure has been identified. The geometry optimizations were carried out for every possible spin state. The spin distribution was studied by using Mulliken population analysis. Note that the Mulliken atomic spin and charge population could vary with the basis set,[30] but previous studies showed that it is appropriate and a widely accepted practice to employ Mulliken population analysis to obtain the atomic spin densities, especially for transition-metal-based systems.[31−36] The threshold for the energy and force convergence was set to 0.00001 and 0.001 eV/Å, respectively.

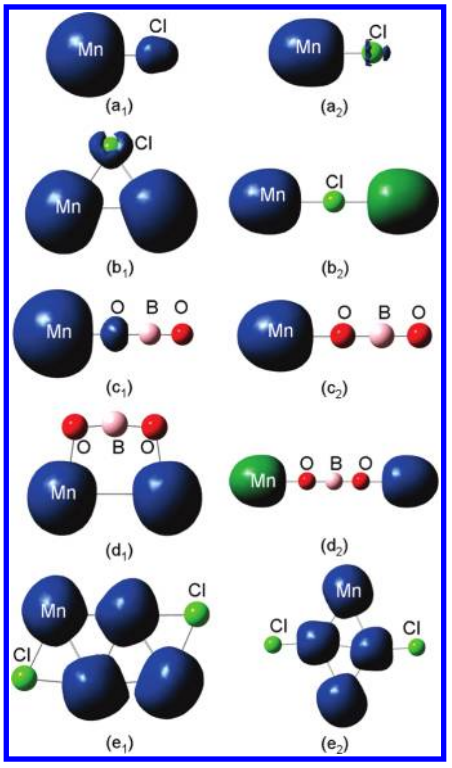

Figure 3. Spin density distribution of (a_1) MnCl, (a_2) $MnCl^-$, (b_1) Mn_2Cl, (b_2) Mn_2Cl^-, (c_1) $MnBO_2$, (c_2) $MnBO_2^-$, (d_1) Mn_2BO_2, (d_2) $Mn_2BO_2^-$, (e_1) $(Mn_2Cl)_2$, and (e_2) $(Mn_2Cl)_2^-$ clusters. The isosurface value is 0.004.

The vibrational frequencies of all the clusters studied are found to be positive suggesting that their geometries are dynamically stable. In the following section we present our results corresponding to the lowest-energy structures and the preferred spin state.

III. RESULTS AND DISCUSSION

A. MnCl and $MnCl^-$. We begin with the results on MnCl. The optimized structure of both the neutral and anionic MnCl, its IP, EA, MM, Mulliken atomic spin density distributions, as well as the charge on each of the atom through natural bond orbital (NBO) analysis were calculated. The results are given in Figure 1 and Table 2. The neutral Mn−Cl bond length of 2.27 Å and the gap of 2.26 eV between the highest occupied molecular orbital (HOMO) and lowest unoccupied molecular orbital (LUMO) are both enlarged to 2.40 Å and 2.55 eV, respectively, in the anion. Since Cl atom has a large electron affinity compared to that of Mn atom, charge is transferred from Mn atom to Cl. This is confirmed by NBO analysis shown in Table 2 for both neutral and anionic MnCl. The HOMO and LUMO are plotted in Figure 2. We note that the HOMO of MnCl is mainly contributed from Cl 2p and the 4s 3d hybridized orbitals of Mn, while the LUMO of MnCl and the HOMO and LUMO of $MnCl^-$ are mostly contributed by the Mn d_{z^2} orbital. The magnetic moment of MnCl and $MnCl^-$ is found to be 6 and 5 μ_B, respectively, which can be qualitatively understood with the following pictures: As Cl draws an electron from the Mn atom, it leaves behind Mn in a positively charged state with an electronic configuration of $3d^5 4s^1$ and hence with a magnetic moment of 6 μ_B. In $MnCl^-$, the extra electron preferentially goes to neutralize

dx.doi.org/10.1021/jp106198u |J. Phys. Chem. A 2011, 115, 549–555

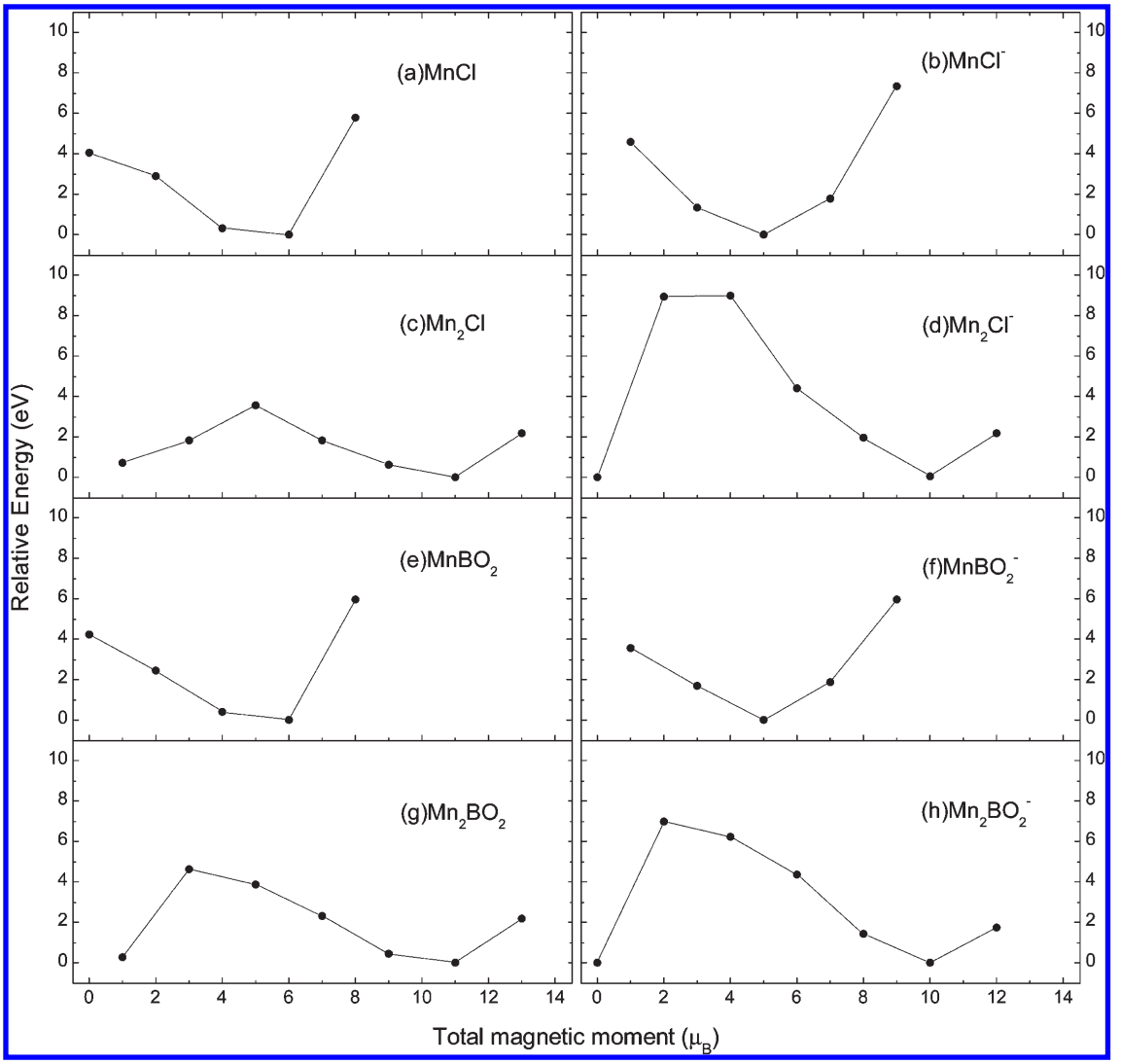

Figure 4. The relative energies of different spin configurations of (a) MnCl, (b) $MnCl^-$, (c) Mn_2Cl, (d) Mn_2Cl^-, (e) $MnBO_2$, (f) $MnBO_2^-$, (g) Mn_2BO_2, and (h) $Mn_2BO_2^-$ measured with respect to their respective lowest-energy spin structure.

the Mn^+ site in MnCl, and the total magnetic moment of $MnCl^-$ reverts back to 5 μ_B. However, due to the partial charge transfer between Mn and Cl (Table 2), Cl is also slightly ferromagnetically polarized with a moment of 0.16 and 0.09 μ_B in MnCl and $MnCl^-$, respectively, as can be seen from the spin density distribution plotted in Figure 3 (a_1 and a_2). The relative energies of MnCl and $MnCl^-$ for different spin states measured with respect to their lowest spin configuration are given in parts a and b of Figure 4.

B. Mn_2Cl and Mn_2Cl^-. We next discuss our results in Mn_2Cl and its anion Mn_2Cl^-. To obtain the equilibrium geometry three different initial structures were chosen, and optimization was performed for every possible spin state to obtain the preferred magnetic moment. The initial structures included a triangle and two linear structures in which the Mn and Cl atoms were placed in the middle position, respectively. For the neutral Mn_2Cl cluster, our fully optimized structure yielded an isosceles triangle (see Figure 1) with a total magnetic moment of 11 μ_B as its lowest-energy configuration. Mn atoms are coupled ferromagnetically. From the Mulliken analysis we find each Mn atom carrying a magnetic moment of 5.44 μ_B. The bond length of 2.84 Å between Mn atoms in Mn_2Cl is very close to the bond length of Mn_2^+. This can be explained through the NBO charge analysis which shows that the Cl atom has negative charge of 0.80 leaving each Mn atom carrying a positive charge of 0.40 (in Table 1). For the anion Mn_2Cl^- cluster we get a linear structure with two Mn atoms in an antiferromagnetically coupled state, each carrying a 5 μ_B magnetic moment. This is consistent with the fact that in Mn_2Cl^- the extra electron resides primarily on the Cl site leaving two Mn atoms in Mn_2Cl^- behave just like they do in neutral Mn_2 which is antiferromagnetic. Note that there is no bond between Mn atoms in Mn_2Cl^- and the bond length between Mn−Cl is 2.58 Å. The relative energies for different spin states measured with respect to the lowest spin configuration are plotted in parts c and d of Figure 4. The HOMO and LUMO orbitals for both of the Mn_2Cl and Mn_2Cl^- are plotted in Figure 5, where the Cl 2p and the hybridized Mn 3d 4s orbitals contribute to the HOMO in Mn_2Cl, while Mn $3d_{z^2}$ orbitals are dominant in the LUMO of Mn_2Cl and in the HOMO and LUMO of Mn_2Cl^-. In particular, the additional electron on Cl makes the Mn_2Cl^- behave as if it is composed of two parts, a $MnCl^-$ part and a Mn part; the HOMO and LUMO of the

dx.doi.org/10.1021/jp106198u |J. Phys. Chem. A 2011, 115, 549–555

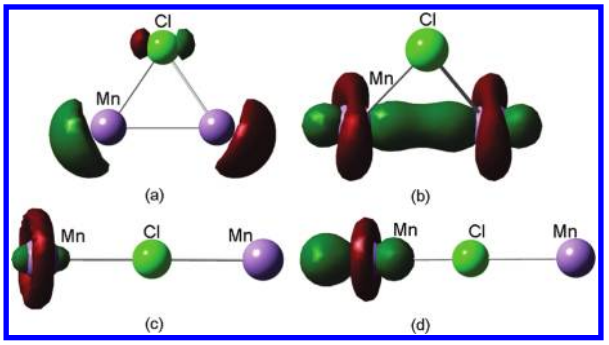

Figure 5. (a) HOMO and (b) LUMO of Mn_2Cl; (c) HOMO and (d) LUMO of Mn_2Cl^-.

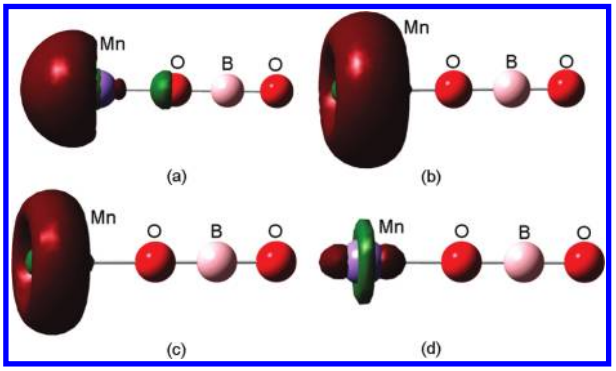

Figure 6. (a) HOMO and (b) LUMO of $MnBO_2$; (c) HOMO and (d) LUMO of $MnBO_2^-$.

$MnCl^-$ parts in Mn_2Cl^- are similar to the HOMO and LUMO of $MnCl^-$ in Figure 3. Thus, we see that Cl is able to change the magnetic coupling between the Mn atoms.

C. $MnBO_2$ and $MnBO_2^-$. BO_2^-, which is isoelectronic with CO_2, is known to be a superhalogen with an electron affinity of 4.8 eV.[11] Since Cl can draw an electron from Mn and cause its magnetic moment to increase, we envisioned that $MnBO_2$ should also behave in a similar way. Following the same procedure as above, we optimized the geometries of both neutral and anion cluster of $MnBO_2$ for all possible spin states. We used four different initial configurations for optimization by placing Mn atom next to B and O atoms as well as connected simultaneously to both the B and O atoms. The lowest-energy structure is similar to that of MnCl. The relative energies of neutral and anionic $MnBO_2$ for different spin states measured with respect to their lowest spin configurations are plotted in parts e and f of Figure 4. The total magnetic moment of the ground state for $MnBO_2$ is 6 μ_B and that for $MnBO_2^-$ is 5 μ_B. Both of them have a linear structure (as shown in Figure 1), and the distance of the Mn−O bond is 1.90 Å for neutral and 2.01 Å for the anion. From the NBO analysis, we see that, in neutral $MnBO_2$, the Mn atom donates 0.89 charge to the BO_2 moiety. When an extra electron is added to $MnBO_2$, it preferentially goes to the Mn site, thus neutralizing its positive charge. The BO_2 moiety in $MnBO_2^-$ carries a negative charge of 0.98. Note that in $MnCl^-$, Cl carried a charge of 0.9. The HOMO and LUMO orbitals are represented in Figure 6, where the orbitals from Mn site are predominant. In comparison to the HOMO and LUMO of $MnBO_2$ and $MnBO_2^-$ with MnCl and $MnCl^-$, we can see that the BO_2 moiety is playing exactly the same role as the Cl atom does in the clusters.

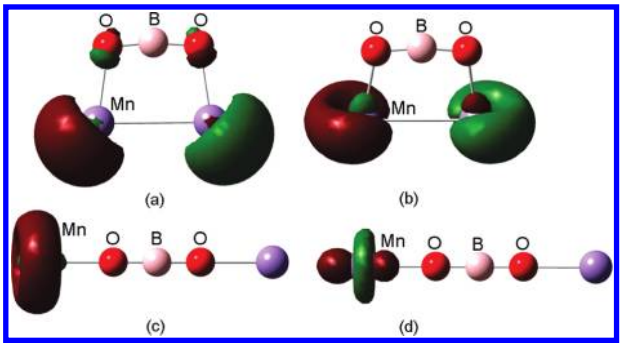

Figure 7. (a) HOMO and (b) LUMO of Mn_2BO_2; (c) HOMO and (d) LUMO of $Mn_2BO_2^-$.

D. Mn_2BO_2 and $Mn_2BO_2^-$. Next we studied the interaction of BO_2 with a Mn_2 dimer. We expected that in analogy with Mn_2Cl Mn_2BO_2 should also be ferromagnetic with a magnetic moment of 11 μ_B. We chose more than 10 initial configurations for geometry optimization by placing the two Mn atoms at different binding sites on the BO_2 moiety. The lowest-energy structures for both the neutral and anion Mn_2BO_2 clusters are shown in Figure 1. The relative energies of neutral and anionic Mn_2BO_2 for different spin states measured with respect to their lowest spin configurations are plotted in parts g and h of Figure 4. The total magnetic moment of the ground state of Mn_2BO_2 is 11 μ_B. As expected, the magnetic coupling in $Mn_2BO_2^-$ is antiferromagnetic, and hence, the total magnetic moment is zero. Thus, one can switch the coupling in Mn_2BO_2 from ferromagnetic to antiferromagnetic simply by adding an electron. We note that the geometries of neutral and anionic Mn_2BO_2 are also similar to those of Mn_2Cl when Cl is replaced by BO_2; the neutral has a triangular structure, while the anion is linear. Because of the large electron affinity of BO_2, 1.16 electrons are transferred from Mn_2 to BO_2 in Mn_2BO_2 cluster (see Table 2) leaving two Mn atoms in a state of Mn_2^+ and ferromagnetically coupled with a Mn−Mn bond length of 3.13 Å. The extra electron in $Mn_2BO_2^-$ anion goes almost entirely to the BO_2 moiety, leaving two Mn atoms as in neutral state of Mn_2 and coupled antiferromagnetically. The HOMO and LUMO orbitals of these two clusters are given in Figure 7. Here again the HOMO and LUMO of Mn_2BO_2 and $Mn_2BO_2^-$ are similar to those of Mn_2Cl and Mn_2Cl^-; the main contributions arising from the Mn orbitals. It is also interesting to note the differences: the LUMO of Mn_2Cl is mainly from the Mn $3d_{z^2}$ orbital of two Mn sites with the same phase (Figure 5b), while the LUMO of Mn_2BO_2 is mainly from the hybridized 3d 4s orbitals of two Mn sites but with different phase (Figure 7b).

E. $(Mn_2Cl)_2$ and $(Mn_2Cl)_2^-$. We have shown in the above that it is possible to induce ferromagnetic transition in Mn_2 dimer by reacting it with a halogen atom such as Cl or superhalogen moiety such as BO_2. In this section we explore the magnetic coupling between Mn spins as two Mn_2Cl units are allowed to form a dimer. We have calculated the equilibrium geometries of both neutral and anionic $(Mn_2Cl)_2$ clusters for all allowable spin configurations. The vertical detachment energies and electron affinities are also calculated so that they can be compared with future experiments to validate the accuracy of our predictions. Several initial configurations were tried to obtain the lowest-energy structure, which is shown in Figure 1. The magnetic moments localized at the Mn sites in both neutral and anionic $(Mn_2Cl)_2$ clusters are coupled ferromagnetically, resulting in

dx.doi.org/10.1021/jp106198u |J. Phys. Chem. A 2011, 115, 549–555

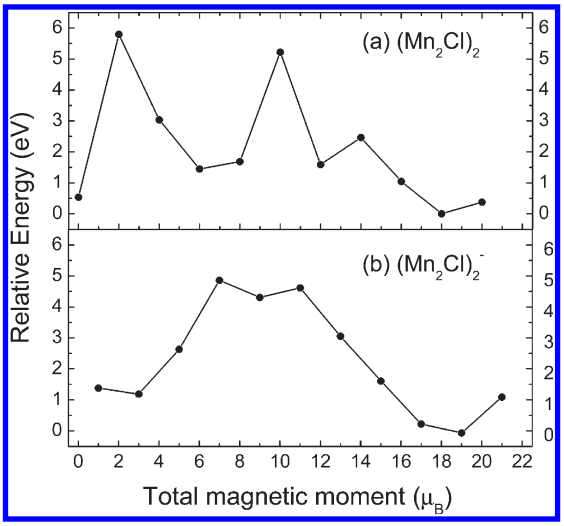

Figure 8. Relative energies of different spin configurations of (a) $(Mn_2Cl)_2$ and (b) $(Mn_2Cl)_2^-$ measured with respect to their lowest-energy spin structure.

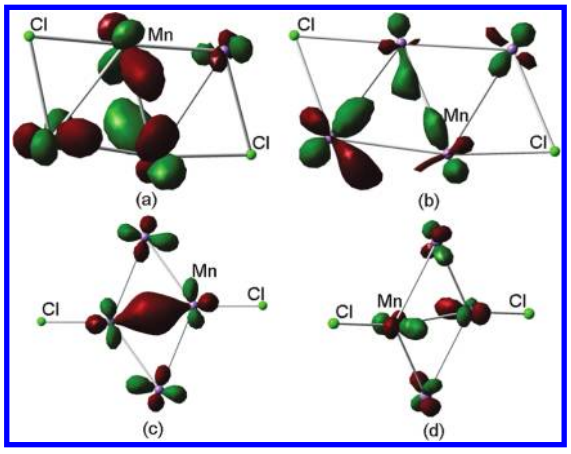

Figure 9. (a) HOMO and (b) the LUMO of $(Mn_2Cl)_2$; (c) HOMO and (d) LUMO of $(Mn_2Cl)_2^-$.

total magnetic moments of 18 μ_B for the neutral and 19 μ_B for the anion. The spin density distribution plotted in Figure 3 (e_1 and e_2) shows that the magnetic moments are primarily concentrated at the Mn sites. The Mulliken atomic spins and NBO charges are given in Table 2. In both of these cases charges are transferred from Mn atoms to Cl atoms. The neutral cluster geometry has C_s symmetry, while the anion has C_{2h} symmetry. The relative energies of each spin state measured with respect to the lowest-energy spin configuration are plotted in parts a and b of Figure 8. The HOMO and LUMO orbitals of the two lowest-energy clusters are shown in Figure 9. The HOMO and LUMO orbitals of these two clusters are mainly from d_{xy}, d_{xz}, d_{yz}, and $d_{x^2-y^2}$ of Mn sites.

IV. CONCLUSION

In summary, by using DFT and B3LYP functional for exchange and correlation potential we have calculated the equilibrium geometries, magnetic couplings, electronic structures, vertical detachment energies, and electron affinities of Mn atoms interacting with Cl and BO_2. We find that halogens and superhalogens have the same effect of accepting electrons to tune the magnetic coupling between Mn atoms, namely, the two Mn atoms in Mn_2Cl and Mn_2BO_2 couple ferromagnetically as they do in Mn_2^+. In contrast, the coupling between Mn atoms in Mn_2Cl^- and $Mn_2BO_2^-$ becomes antiferromagnetic such as what happens in neutral Mn_2. Almost all the magnetic moments are localized at the Mn site. We also find that when two Mn_2Cl clusters are allowed to interact with each other the resulting Mn_4Cl_2 cluster remains ferromagnetic with a total magnetic moment of 18 μ_B. Here all four Mn atoms cluster to form a rhombuslike structure with the two Cl atoms removed to either end of the cluster. We have also calculated the electron affinities of these clusters, which can be compared with experimental data when available. We hope that this paper will stimulate photoelectron spectroscopy experiments so that our predictions can be verified. In addition, using chemical reaction to promote magnetic transition can be used as another means to synthesize new magnetic materials.

AUTHOR INFORMATION

Corresponding Author
*E-mail: pjena@vcu.edu.

ACKNOWLEDGMENT

This work is supported in part by grants from the Department of Energy, the China Scholarship Council, and the National Natural Science Foundation of China (NSFC-10744006). This research used resources of the National Energy Research Scientific Computing Center, which is supported by the Office of Science of the U.S. Department of Energy under Contract No. DE-AC02-05CH11231.

REFERENCES

(1) Morse, M. D. *Chem. Rev.* **1986,** *86,* 1049.
(2) Asada, T.; Terakura, K. *Phys. Rev. B* **1993,** *47,* 15992.
(3) Chu, D; Kenning, C. G.; Orbach, R *Phys. Rev. Lett.* **1994,** *72,* 3270.
(4) Baumann, C. A.; Van Zee, R. J.; Bhat, S. B.; Weltner, W. *J. Chem. Phys.* **1983,** *78,* 190.
(5) Van Zee, R. J.; Weltner, W, Jr. *J. Chem. Phys.* **1988,** *89,* 4444.
(6) Cheeseman, M.; Van Zee, R. J.; Flanagan, H. L.; Weltner, W., Jr. *J. Chem. Phys.* **1990,** *92,* 1553.
(7) Tono, K.; Terasaki, A.; Ohta, T; Kondow, T. *J. Chem. Phys.* **2005,** *123,* 174314.
(8) Nayak, S. K.; Nooijen, M.; Jena, P. *J. Phys. Chem. A* **1999,** *103,* 9853.
(9) Knickelbein, M. *Phys. Rev. Lett.* **2001,** *86,* 5255. Khanna, S. N.; Rao, B. K.; Jena, P.; Knickelbein, M. *Chem. Phys. Lett.* **2003,** *378,* 374.
(10) Nayak, S. K.; Rao, B. K.; Jena, P. *J. Phys.: Condens. Matter* **1998,** *10,* 10863.
(11) Nayak, S. K.; Jena, P. *Chem. Phys. Lett.* **1998,** *289,* 473.
(12) Lau, J. T.; Hirsch, K.; Langenberg, A.; Probst, J.; Richter, R.; Rittmann, J.; Vogel, M.; Zamudio-Bayer, V.; Möller, T.; von Issendorff, B. *Phys. Rev. B* **2009,** *79,* 241102.
(13) Terasaki, A.; Matsushita, A.; Tono, K.; Yadav, R. T.; Briere, T. M.; Kondow, T. *J. Chem. Phys.* **2001,** *114,* 9367.
(14) Zhai, H. J.; Wang, L. M.; Li, S. D.; Wang, L. S. *J. Phys. Chem. A* **2007,** *111,* 1030.
(15) Gutsev, G. L.; Boldyrev, A. I. *Chem. Phys.* **1981,** *56,* 277.
(16) George, C.; Mayne, F.; Prigogine, I. *Adv. Chem. Phys.* **1985,** *61,* 223.
(17) Lee, C. T.; Yang, W. T.; Parr, R. G. *Phys. Rev. B* **1988,** *37,* 785.

(18) Becke, A. D. *J. Chem. Phys.* **1993,** *98*, 1372.
(19) Becke, A. D. *J. Chem. Phys.* **1993,** *98*, 5648.
(20) Frisch, M. J.; Trucks, G. W.; Schlegel, H. B.; Scuseria, G. E.; Robb, M. A.; Cheeseman, J. R.; Montgomery, J. A., Jr.; Vreven, T.; Kudin, K. N.; Burant, J. C.; Millam, J. M.; Iyengar, S. S.; Tomasi, J.; Barone, V.; Mennucci, B.; Cossi, M.; Scalmani, G.; Rega, N.; Petersson, G. A.; Nakatsuji, H.; Hada, M.; Ehara, M.; Toyota, K.; Fukuda, R.; Hasegawa, J.; Ishida, M.; Nakajima, T.; Honda, Y.; Kitao, O.; Nakai, H.; Klene, M.; Li, X.; Knox, J. E.; Hratchian, H. P.; Cross, J. B.; Bakken, V.; Adamo, C.; Jaramillo, J.; Gomperts, R.; Stratmann, R. E.; Yazyev, O.; Austin, A. J.; Cammi, R.; Pomelli, C.; Ochterski, J. W.; Ayala, P. Y.; Morokuma, K.; Voth, G. A.; Salvador, P.; Dannenberg, J. J.; Zakrzewski, V. G.; Dapprich, S.; Daniels, A. D.; Strain, M. C.; Farkas, O.; Malick, D. K.; Rabuck, A. D.; Raghavachari, K.; Foresman, J. B.; Ortiz, J. V.; Cui, Q.; Baboul, A. G.; Clifford, S.; Cioslowski, J.; Stefanov, B. B.; Liu, G.; Liashenko, A.; Piskorz, P.; Komaromi, I.; Martin, R. L.; Fox, D. J.; Keith, T.; Al-Laham, M. A.; Peng, C. Y.; Nanayakkara, A.; Challacombe, M.; Gill, P. M. W.; Johnson, B.; Chen, W.; Wong, M. W.; Gonzalez, C.; Pople, J. A. *Gaussian 03*, revision B.04; Gaussian, Inc.: Wallingford, CT, 2004.
(21) Perdew, J. P.; Chevary, J. A.; Vosko, S. H.; Jackson, K. A.; Pederson, M. R.; Singh, D. J.; Fiolhais, C. *Phys. Rev. B* **1992,** *46*, 6671.
(22) Perdew, J. P.; Burke, K.; Ernzerhof, M. *Phys. Rev. Lett.* **1996,** *77*, 3865.
(23) Perdew, J. P.; Wang, Y. *Phys. Rev. B* **1992,** *45*, 13244.
(24) Stephens, P. J.; Devlin, F. J.; Chabalowski, C. F.; Frisch, M. J. *J. Phys. Chem.* **1994,** *98*, 11623.
(25) Ruiz, E.; Alemany, P.; Alvarez, S.; Cano, J. *J. Am. Chem. Soc.* **1997,** *119*, 1297.
(26) Sinnecker, S.; Neese, F.; Noodleman, L.; Lubitz, W. *J. Am. Chem. Soc.* **2004,** *126*, 2613.
(27) Ruiz1, E.; Alvarez1, S.; Cano, J.; Polo, V. *J. Chem. Phys.* **2005,** *123*, 164110.
(28) Rivero, P.; Moreira, I. de P. R.; Illas, F.; Scuseria, G. E. *J. Chem. Phys.* **2008,** *129*, 184110.
(29) Peralta, J. E.; Melo, J. I. *J. Chem. Theory Comput* **2010,** *6*, 1894.
(30) Philips, J. J.; Hudspeth, M. A.; Browne, P. M., Jr.; Peralta, J. E. *Chem. Phys. Lett.* **2010,** *495*, 146.
(31) Blomberg, M. R. A.; Siegbahn, P. E. M. *Theor. Chem. Acc.* **1997,** *97*, 72.
(32) Chartier, A.; D'Arco, P.; Dovesi, R.; Saunders, V. R. *Phys. Rev. B* **1999,** *60*, 14042.
(33) Siegbahn, P. E. M. *Curr. Opin. Chem. Biol.* **2002,** *6*, 227.
(34) Huang, Z. F.; Wang, C. Z.; Meng, X.; Wang, D. P.; Chen, G. *J. Solid State Chem.* **2006,** *179*, 1602.
(35) Privalov, T.; Sun, L.; Åkermark, B.; Liu, J.; Gao, Y.; Wang, M. *Inorg. Chem.* **2007,** *46*, 7075.
(36) Quiñonero, D.; Musaev, D. G.; Morokuma, K. *THEOCHEM* **2009,** *903*, 115.